Iranian Journal of Science & Technology, Transaction B, Engineering, Vol. 32, No. B2, pp 107-124
Printed in The Islamic Republic of Iran, 2008

SEISMIC 3D BEARING CAPACITY ANALYSIS OF SHALLOW FOUNDATIONS*

A. R. MAJIDI AND A. A. MIRGHASEMI**

School of Civil Engineering, College of Engineering, University of Tehran P.O. Box 11155-4563, I. R. of Iran
Email: aghasemi@ut.ac.ir

Abstract– In this research the Discrete Element Method is employed to determine the seismic three dimensional bearing capacity of rectangular foundations. A rigid but moving slip body resting on its base is assumed to define the failure mechanism under the footing. A soil mass enclosed in a three dimensional space with assumed failure surfaces is considered as several discrete blocks connected with Winkler springs. The geometry of the failure surface under the foundation is not fixed and can be altered due to all of the factors affecting the problem. This geometry is determined by six independent angles. The seismic loading can be applied to the soil mass, soil surcharge and foundation loading in a pseudo-static manner. This paper includes the derivation of 3D DEM formulation in a three dimensional state, and several examples solved by means of a developed DEM program to explain the capability of the method and to compare the results with the other methods.

Keywords– 3 Dimensional, bearing capacity, shallow foundations/footings, seismic, pseudo-static, discrete element method

1. INTRODUCTION

The bearing capacity of foundations has always been one of the most interesting sources of research in geotechnical engineering with numerous published papers and reports. Among these, extensive studies have been made for two dimensional problems of strip footing which rest on a horizontal or inclined slope surface. In this regard, different methods of analysis are introduced. It seems that 2D theoretical approaches have reached a relatively satisfactory level for ordinary loading and soil conditions. However, three dimensional problems of bearing capacity, even in static loading conditions, still require more experimental and theoretical research activities.

In static conditions, the evaluation of the 3D bearing capacity of shallow foundations is usually assessed by introducing experimental and empirical shape factors into the ordinary 2D equations for the strip footings developed by earlier researchers such as Meyerhof [1], Terzaghi and Peck [2], Hansen [3], de Beer [4], Vesic [5], etc. These empirical shape factors are commonly based on the test results obtained from the works of Golder [6] and some additional unpublished data.

Shield and Drucker [7], for the first time, attempted a theoretical evaluation of the bearing capacity of rectangular foundations on homogeneous clay ($\phi = 0$) by means of upper and lower bound solutions. Also, the theoretical analyses of the bearing capacity of circular footings have been done by Kötter's equation in the state of rigid plasticity [8, 9]. Nakase [10] used an ordinary limit equilibrium method and assumed cylindrical sliding surfaces in rectangular footings on normally consolidated clays, of which strength

*Received by the editors May 15, 2006; final revised form October 15, 2007.
**Corresponding author

increases linearly with depth. Ugai [11] presented more rigorous solutions for rectangular foundations on NC clays with the help of limit analysis, by improving the admissible velocity field originally proposed by Shield and Drucker [7] to include the effect of the roughness of the footing base. Narita and Yamaguchi [12] presented a three dimensional analysis of the bearing capacity of rectangular foundations by means of the slices method, assuming that sliding surfaces are composed of a set of log-spiral with different initial radii in the direction of the longer axis of the footing base. Michalowski [13] introduced a 3D analysis of rectangular foundations based on the limit analysis (upper-bound) approach, in which all mechanism of failure considered in the analysis consisted of four regions, each characterized by plane deformations. Michalowski and Dawson [14] then compared the results of the suggested upper bound method with the numerical results of the FLAC^{3D} code. Also, Zhu and Michalowski [15] calculated the shape factors for square and rectangular footings which are based on the proposed upper bound method and compared them with finite element analysis results. Salgado *et al*. [16] calculated, rigorously, the bearing capacity of strip, square, circular and rectangular foundations in clay, based on the finite element limit analysis.

For strip foundations (2D state), incorporating the effects of earthquake body forces, investigations have been performed by using the method of inclined slices [17] limit equilibrium [18], and the upper bound limit analysis [19-22]). Kumar and Mohan Rao [23] have computationally examined the effect of horizontal earthquake body forces on the bearing capacity of 2D foundations in a rigorous manner by employing the method of stress characteristics. Ghahramani and Berrill [24] also evaluated the seismic bearing capacity factors by the zero extension method, which is first proposed by Roscoe [25].

Experimental and theoretical investigations have both clearly demonstrated that the bearing capacity of foundations substantially reduces during earthquakes. Unfortunately, no theoretical solution for 3D bearing capacity in seismic conditions have been offered so far and very limited information is available to predict the 3D behaviour of foundations during an earthquake.

Different investigators have used different methods of analysis in their studies. Among these methods, limit equilibrium, limit analysis and continuum based methods such as finite element and finite difference methods are widely used. Calculations based on the limit equilibrium method for the problem of bearing capacity generally do not satisfy all equilibrium conditions; therefore, additional assumptions are required with respect to interslice forces and stresses. The finite element method or finite difference method, require information about the initial stress state existing in the soil, a correct constitutive model and correct parameters for the constitutive model. Implementation of these requirements increases the complexity of the analysis and the probability of uncertainty in the results. Also, such an analysis is often quite time consuming and achieving the convergence of results becomes a difficult task.

The new concept of discrete element method (DEM), which falls within the framework of the limit equilibrium methodology, in a two dimensional state, was presented by Chang for the bearing capacity of foundations [26], slope stability [27] and the retaining wall [28]. In this new concept of DEM, instead of modeling individual particles, he considered a soil mass as several discrete blocks connected with Winkler springs. By developing the concept proposed by Chang [26-28], a three dimensional formulation of the discrete element method were presented by the authors [29, 30]. Mirghasemi and Maleki-Javan also used this method to analyze the Retaining Wall Earth Pressure in Static and Pseudo-Static Conditions [31]. In this paper, for the first time, an effort is made to determine the seismic three dimensional bearing capacity of rectangular foundations using DEM. Several tables and graphs are provided to demonstrate the applicability of this method. The computations in this research are carried out by means of a developed DEM program named BCAP^{3D}, (Bearing Capacity Analysis Program in 3 Dimension), written in MATLAB.

2. DISCRETE ELEMENT MODEL

To determine three dimensional bearing capacity of rectangular shallow foundations by DEM, a rigid but moving slip body resting on its base is assumed to define the failure mechanism under the footing. The soil mass enclosed in a three dimensional space with assumed failure surfaces is considered as several discrete blocks are connected with Winkler springs, as shown in Fig. 1.

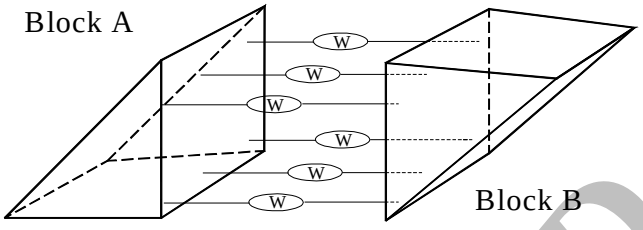

Fig. 1. Connection of adjacent blocks with Winkler springs in 3 dimensional state

Each group of Winkler springs consists of three sets of springs at different orthogonal directions. One set of springs is located in the direction normal to the contact surface in order to simulate the normal stiffness, and the two other sets are placed within the contact surface perpendicular to each other to simulate the shear resistance on all interfaces, as shown in Fig. 2. Therefore, compared to the 2D model, there is one set of shear springs added in the contact surface between two adjacent blocks.

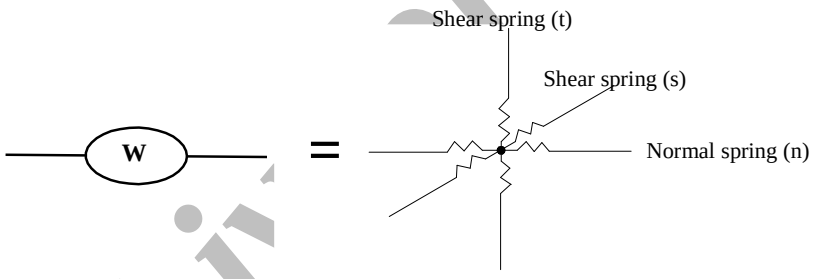

Fig. 2. Winkler spring in 3 dimensional state

The behaviour of the normal and tangent springs is assumed to be Elasto-Plastic. As shown in Fig. 3, the normal springs do not yield in compression, but in tension they would yield at the tensile capacity of F_t, as:

$$F_t = \frac{2c.\cos\varphi}{1+\sin\varphi} \tag{1}$$

where (c) is cohesion and (ϕ) is the internal friction angle of the soil. Also, based on Mohr-Coulomb failure criteria, the shear springs yield when the shear strength (τ_p) is reached, as:

$$\tau_p = c + \sigma_n \,.\, \tan\phi \tag{2}$$

When stresses in the normal or shear springs exceed their final strength, springs yield. In order to reduce the stiffness of yielded springs, the secant method is applied. Regarding the stress-strain relationship as shown in Fig. 3, the initial normal stiffness (k_{normal}) alters to secant normal stiffness (k'_{normal}). With the same concept, the initial shear stiffness (k_{shear}) is substituted by the secant normal stiffness (k'_{shear}).

The Newton-Rophson iterative scheme is applied for modeling nonlinearity properties in plastic conditions. In this iterative scheme, an approximation to the exact stress-strain curve is made based on the slope at the start of the increment, but using an iterative procedure in which the stiffness is updated at each

iteration, the approximation gets refined. The reduced stiffness is obtained using stress divided by strain at each iteration.

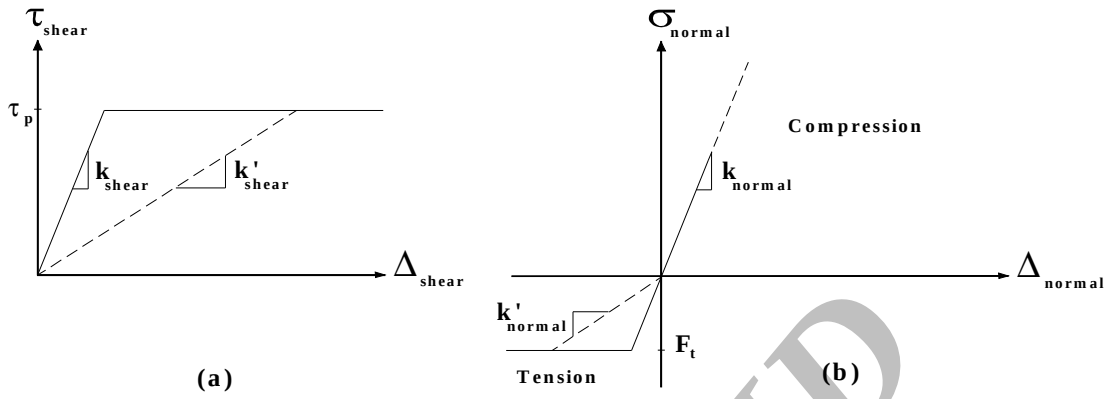

Fig. 3. Stress-Strain behaviour of Winkler springs, a) shear springs, b) normal springs

The initial values of stiffness in the normal and shear directions between blocks can be estimated through their relation with the values of Young's modulus (E) and shear modulus (G), respectively. For isotropic elastic materials, the ratio of (E / G) is given by 2(1+ν), in which ν is the Poission's ratio and varies from 0 to 0.5 for different kinds of soils. Thus, the practical range of (k_{normal} / k_{shear}) is from 2 to 3. It is found that the results in the present method depend on the Winkler spring constants ratio (k_{normal} / k_{shear}) rather than their individual values. Also, the values of (k_{normal} / k_{shear}) in the above mentioned range have an insignificant effect on the computed results [26].

3. FAILURE SURFACE GEOMETRY

In this model, for discretizing the assumed failure surface, pentahedron wedges are used as shown in Fig. 4. Similar to the previous bearing capacity approaches described by some authors [29, 30, 32], the failure mechanism contains an active zone, blow the footing (zone I), which is pushed downward into the soil mass and a passive wedge (zone III) moves laterally. The transition between the downward movement of the active zone and the lateral movement of the passive zone takes place through the radial shear zone (II). The shape of the failure surface of zone (II) is assumed logarithmic spiral. These three regions can be divided into any arbitrary number of blocks, e.g. N_1, N_2 and N_3, respectively. The geometry of the failure surface is a function of the footing width (B) and length (L), internal friction angle of the underneath soil (ϕ), and the six independent angles of α_1, α_2, α_3, α_4, θ_1 and θ_2.

The angles θ_1 and θ_2 determine the inclination of lateral failure surfaces in a three dimensional space. The absolute values of θ_1 and θ_2 are assumed identical ($|\theta_1| = |\theta_2|$). As shown in Fig. 5, if the lateral failure surfaces incline inward or outward, θ_1 and θ_2 possess negative or positive values, respectively. The zero value for these angles indicates that lateral failure surfaces are vertical. However, unlike the classical limit methods, there is no special pre-assumption in the determination of the failure surface's angles (including θ_1 and θ_2). These six angles are found by a trial and error procedure to obtain the minimum ultimate bearing capacity. The result of the calculation procedure for a certain shallow foundation indicates which mode of side surface geometry (Fig. 5) governs the problem.

Due to the existence of six independent angles, a very extensive number of failure surfaces are examined to determine the minimum bearing capacity. Therefore, with more complex failure surface

geometry, the accuracy of the solution is improved in comparison with simpler failure surfaces geometry, commonly considered in classical limit equilibrium or limit analysis methods.

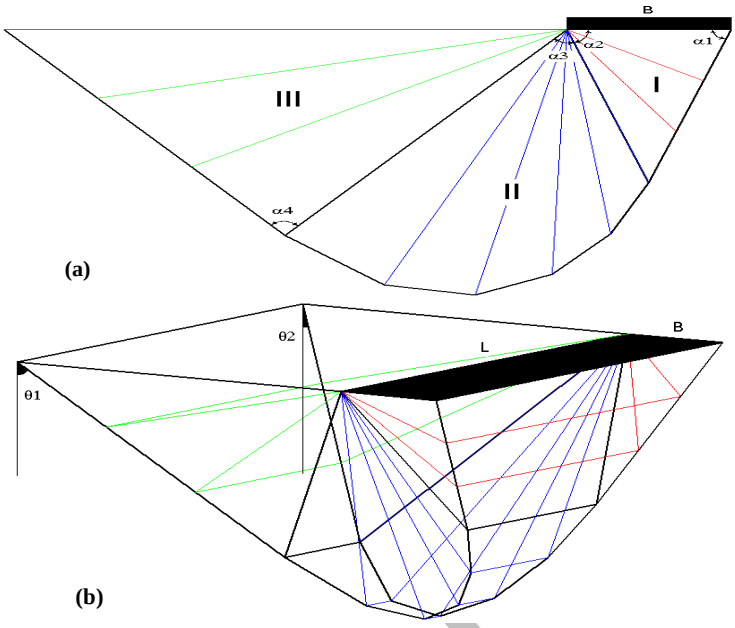

Fig. 4. Aspect of failure surface geometry, a) 2D view, b) 3D view

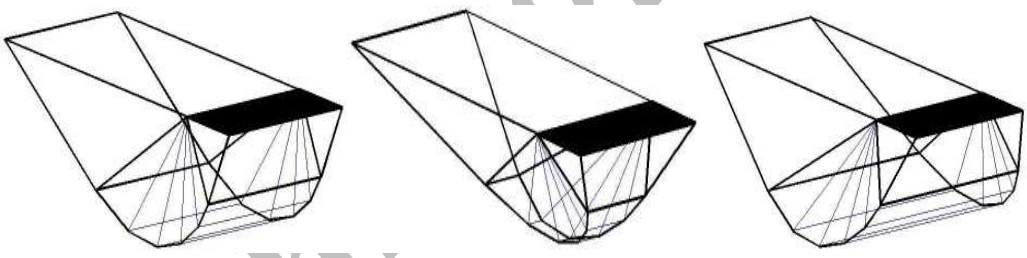

(a) (b) (c)

Fig. 5. The inclination of lateral failure surfaces in three dimensional space, a) zero value for θ_1 and θ_2 (vertical), b) negative value (inclined inward), c) positive value (inclined outward)

4. 3D FORMULATION

To obtain the three dimensional formulation of DEM, it is assumed that each block is rigid and only relative displacements of adjacent blocks are taken into consideration. Also, in comparison with relative translation, the relative rotation of two neighbouring blocks is small. Therefore, due to the fact that the two adjacent blocks remain in contact and no separation occurs at contact surfaces under the relative displacement, the continuum theorem can be applied to show the discontinuous deformations in the studied media.

In Fig. 6a, consider two blocks A and B, which are connected together in (x,y,z) space before displacement. After loading, two contacting blocks are moved and exaggeratedly illustrated as separate (Fig. 6b).

Let U_i^a and U_i^b represent the translation and rotation of the displacement vector of blocks A and B, respectively (i=1,2,…,6). These vectors in (x,y,z) space contain six components, where three elements (U_1,U_2,U_3) represent translations in (x,y,z) directions and the other three elements (U_4,U_5,U_6) represent

rotations around this axis. Let point P be the centre of the interface surface between these two blocks. The displacement of block B relative to block A at point P is then expressed as follows:

$$\{ \Delta P_{x,y,z} \} = [R^{b}_{p}] \{ U^{b} \} - [R^{a}_{p}] \{ U^{a} \} \quad (3)$$

where $[R^{a}_{p}]$ is the matrix joining the centroid of the block A to point P. If, however block B is fixed, the values of U_i^b are taken as zero. The displacement vector on the left side of Eq. (3) can be transformed from an (x,y,z) coordinate to the local (n,s,t) coordinate, which n_i^p is an outward unit vector normal to the side face of block A at point P as follows:

$$\{ \Delta P_{n,s,t} \} = [T] \{ \Delta P_{x,y,z} \} \quad (4)$$

where [T] is the transformation orthogonal matrix ($T^{T}_{ij} = T^{-1}_{ij}$). Due to the relative translations and rotations between the two neighbouring blocks, the springs are deformed and the normal and shear stresses are created on the interface surfaces. Therefore, at any point P' on the interface, the springs' deformation in normal ($\Delta_n P'$) and in shear directions ($\Delta_s P', \Delta_t P'$) can be obtained by:

$$\Delta_n P' = \Delta_n P + \Delta_t w.s_{P'} + \Delta_s w.t_{P'} \quad (5.1)$$

$$\Delta_s P' = \Delta_s P + \Delta_n w.t_{P'} \quad (5.2)$$

$$\Delta_t P' = \Delta_t P + \Delta_n w.s_{P'} \quad (5.3)$$

where ($\Delta_n w, \Delta_s w, \Delta_t w$) are the relative rotational components of the displacement vector in local coordinates. Also, $s_{P'}$ and $t_{P'}$ are the distance of point P' from point P on the interface in s and t directions, respectively. That is to say, the total stress distribution on the interface surface due to relative displacement can be divided as:

(a) Uniform normal stress distribution, due to the relative translation of the centres of the interface surfaces of two adjacent blocks, in the direction of n axis ($\Delta_n P$).
(b) Triangular normal stress distribution, due to the relative rotation of two adjacent blocks, around the s axis ($\Delta_s w.t_{P'}$).
(c) Triangular normal stress distribution, due to the relative rotation of two adjacent blocks, around the t axis ($\Delta_t w.s_{P'}$).
(d) Uniform shear stress distribution, due to the relative translation of two adjacent blocks, in the direction of the s axis ($\Delta_s P$).
(e) Uniform shear stress distribution, due to the relative translation of two adjacent blocks, in the direction of the t axis ($\Delta_t P$).
(f) Nonuniform shear stress distribution in the direction of the s axis, due to the relative rotation of two adjacent blocks, around the n axis ($\Delta_n w.t_{P'}$).
(g) Nonuniform shear stress distribution in the direction of the t axis, due to the relative rotation of two adjacent blocks, around the n axis ($\Delta_n w.s_{P'}$).

To obtain the equivalent forces (F_n, F_s, F_t) and moments (M_n, M_s, M_t) in point P, these stresses can be integrated on the interface surface as follows:

$$F_n^p = \iint k_n \cdot \Delta_n P \cdot dA + \iint k_n \cdot s_{P'} \cdot \Delta_t w \cdot dA + \iint k_n . t_{P'} \cdot \Delta_s w \cdot dA \quad (6.1)$$

$$F_s^p = \iint k_s \cdot \Delta_s P \cdot dA + \iint k_s . t_{P'} \cdot \Delta_n w \cdot dA \quad (6.2)$$

$$F_t^p = \iint k_t \cdot \Delta_t P \cdot dA + \iint k_t . s_{P'} \cdot \Delta_n w \cdot dA \quad (6.3)$$

$$M_n^p = \iint \left(k_s \cdot \Delta_s P \cdot t_{P'} + k_s \cdot \Delta_n w \cdot t_{P'}^2\right) dA + \iint \left(k_t \cdot \Delta_t P \cdot s_{P'} + k_t \cdot \Delta_n w \cdot s_{P'}^2\right) dA \quad (6.4)$$

$$M_s^p = \iint k_n \cdot \Delta_n P \cdot t_{P'} \cdot dA + \iint k_n \cdot \Delta_t w \cdot s_{P'} \cdot t_{P'} \cdot dA + \iint k_n \cdot \Delta_s w \cdot t_{P'}^2 \cdot dA \quad (6.5)$$

$$M_t^p = \iint k_n \cdot \Delta_n P \cdot s_{P'} . dA + \iint k_n \cdot \Delta_s w \cdot t_{P'} \cdot s_{P'} \cdot dA + \iint k_n \cdot \Delta_t w \cdot s_{P'}^2 \cdot dA \quad (6.6)$$

where k_n, k_s and k_t are the stiffness coefficients for a unit surface area of normal and shear springs in (n,s,t) directions, respectively.

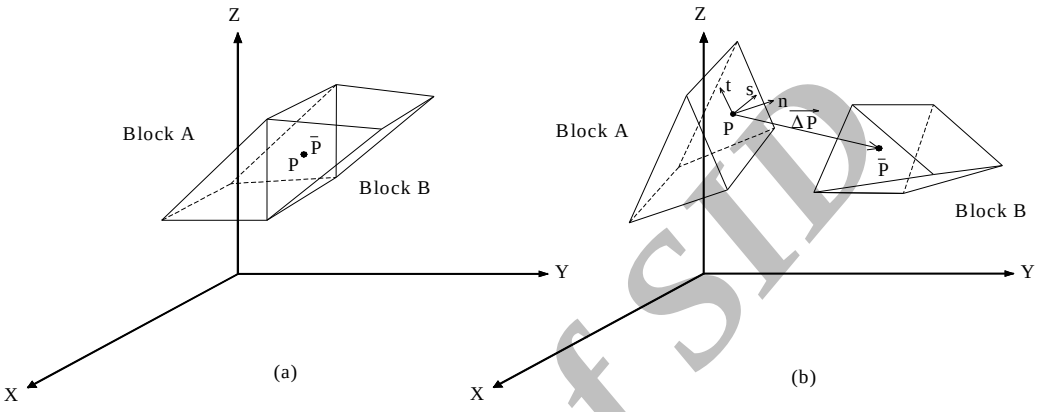

Fig. 6. Displacement of adjacent blocks in 3 dimensional state, a) before and, b) after displacement

Since the relative rotation of two adjacent blocks is considered small, it can be assumed that the spring's coefficients k_n, k_s and k_t are constant in Eq. (6). As a result, similar conditions (elastic or plastic) exist for all springs located at the same direction across the contact surface. The integrals of Eq. (6) can be obtained from ordinary surface inertial moment equations. Then, Eq. (6) can be expressed as:

$$\{ F^P_{n,s,t} \} = [k] \{ \Delta P_{n,s,t} \} \quad (7)$$

where [k] is the stiffness matrix of the associated surface. For convenience, the interface forces in the local coordinate are transformed to the global coordinate by:

$$\{ F^P_{x,y,z} \} = [T]^T \{ \Delta F_{n,s,t} \} \quad (8)$$

From Eqs. (3), (4), (7) and (8), the forces acting on all (n) sides of a block should satisfy the force and displacement equilibrium requirement given by:

$$\{ f^a \} = \sum_{P=1}^{n} -[R^a_p]^T [T^a_p]^T [k^a_p] [T^a_p] [R^b_p] \{U^b\} + [R^a_p]^T [T^a_p]^T [k^a_p] [T^a_p] [R^a_p] \{U^a\} \quad (9)$$

where $\{f^a\}$ is the body force vector in the centroid of block A. In contrast to the finite element method, in which the constraint information is given on nodes, in DEM it is given on the centres of blocks. Based on Eq. (9), the relationship between the forces and the displacements for all blocks can be written as follows:

$$\{ \mathbf{f} \} = [\mathbf{K}] \{ \mathbf{U} \} \quad (10)$$

where [**K**] is the global stiffness of the system and the vectors {**f**} and {**U**} consist of body forces and displacements for all blocks, respectively.

In Eq. (10), there are twelve variables for each block; the body forces vector (f^a_x,f^a_y,f^a_z,m^a_x,m^a_y,m^a_z) and the displacement vector (u^a_x,u^a_y,u^a_z,w^a_x,w^a_y,w^a_z). Body forces are known, thus the 6N simultaneous equations for a system of N blocks can be solved for 6N unknown variables. The relative displacement of

two adjacent blocks can be determined by Eq. (3). The normal and shear forces between blocks can be obtained from Eqs. (4) and (7). Also, the local (L.F.S) and overall (O.F.S) factors of safety can be evaluated by the ratio of shear strength force to shear force on local and overall failure surface, respectively from:

$$\text{L.F.S} = \frac{\tau_p . A}{\sqrt{(\tau_s)^2 + (\tau_t)^2}\, A} \tag{11.1}$$

$$\text{O.F.S} = \frac{\sum \tau_{pi} . A_i}{\sum \sqrt{(\tau_{si})^2 + (\tau_{ti})^2}\, A_i} \tag{11.2}$$

where τ_{si}, τ_{ti} and τ_{pi} are the shear stresses on the failure surface in the directions of s and t and shear strength, respectively.

5. SEISMIC LOADING

Considering the effect of earthquakes horizontal acceleration on vertical center loads is a usual way in limit state methods for evaluating the bearing capacity of foundations. In this way the effects of the inclination of the loads are simply included in the computation procedure.

Pseudo-static dynamic analysis provides an easy way to estimate the bearing resistance of foundations for any imposed earthquake acceleration. In such a methodology the earthquake body forces are incorporated into gravity forces. Here, as a pseudo-static manner, the effects of the earthquake horizontal acceleration (k_h) are applied to the soil weight, soil surcharge and the foundation vertical load, simultaneously.

One of the important advantages of DEM is that the different loading and soil parameters can be simultaneously applied in a single analysis to find the critical failure surface that offers the minimum bearing capacity. The loading system may consist of soil weight, soil surcharge, foundation vertical load and the effect of seismic loading. Therefore, the unique critical failure surface related to all of these parameters is obtained and the accuracy of the solution is improved in comparison with conventional methods, in which the method of superposition is used. In the superposition method, e.g. Terzaghi method [33], the critical failure surfaces related to each parameter are obtained separately.

6. RESULTS

a) Comparison with other methods

Bearing capacity estimation is generally based on the superposition method proposed by Terzaghi [33], in which the contribution of different loading and soil parameters including self weight (γ), internal friction angle (ϕ), surface surcharge (q), and cohesion (c), are expressed in the form of non-dimensional bearing capacity coefficients as follows:

$$q_{ult.} = 0.5B\gamma N'_\gamma + qN'_q + cN'_c \tag{12}$$

where three dimensional bearing capacity coefficients (N'_γ, N'_q and N'_c related to soil weight, surcharge and cohesion, respectively) include the related shape factors (s_γ, s_q, s_c) in the form of:

$$N'_\gamma = s_\gamma N_\gamma \tag{13.1}$$

$$N'_q = s_q N_q \tag{13.2}$$

$$N'_c = s_c N_c \tag{13.3}$$

in which N_γ, N_q and N_c are the ultimate bearing capacity coefficients for a strip foundation in a 2D state.

In classical limit methods, the exact values of surcharge and cohesion bearing capacity coefficients are often obtained by assumption or by derivation and usually fixed at ($\alpha_1 = \alpha_2 = \pi/4 + \phi/2$), ($\alpha_3 = \pi/2$) and ($\alpha_4 = \pi/2 + \phi$) from:

$$N_q = tg^2(\frac{\pi}{4} + \frac{\varphi}{2}) \exp(\pi tg\varphi) \tag{14}$$

$$N_c = (\frac{N_q - 1}{tg\,\varphi}) \tag{15}$$

However, in the present method these critical angles are not predefined and are found by a trial and error procedure. To compute the cohesion coefficient (N'_c or N_c) in DEM, the unit weight of the soil and the load surcharge are set to zero and c = 9.81 kPa. By assuming $\gamma = 0$, c = 0 and q = 9.81 kPa, the N'_q or N_q are calculated. On the other hand, by assuming c = 0, q = 0 and $\gamma = 19.61$ kN/m^3, the N'_γ or N_γ are obtained. The width of footing (B) and the Winkler spring constant ratio (E/G) are assumed 1 m and 2.7, respectively. Also, for obtaining greater accuracy, the number of blocks in zones (I), (II) and (III) is chosen to be 1, 25 and 1, respectively in all computations. In order to make the 3D DEM results comparable to the 2D available solutions, the footing aspect ratio (L/B) was set equal to 1000.

In Figs. 7 and 8, the values of N_q and N_c, obtained respectively by Eqs. (14) and (15), are compared with the results of 3D DEM in two conditions of classical failure with an assumption of ($\alpha_1 = \alpha_2 = \pi/4 + \phi/2$), ($\alpha_3 = \pi/2$) and ($\alpha_4 = \pi/2 + \phi$), and a critical failure surface corresponding to the minimum bearing capacity. As can be seen, the N_q and N_c values obtained from Eqs. (14) and (15) are almost identical to the DEM results with a classical failure surface assumed. However, the critical values of N_q and N_c in DEM, corresponding to the critical failure surface, are obviously less than the classical exact values for ϕ greater than 30°. The reason is that in a limit equilibrium method, we are always looking for the most critical failure surface to get the least bearing capacity.

On the other hand, the values of N_γ obtained from various methods and 3D DEM are compared in Fig. 9. From this comparison, it is concluded that the values of N_γ obtained by 3D DEM are very close to the results of the Vesic [5] method. These differences in various methods are not surprising. For instance, Bowles [34] suggests that for $\phi = 40°$, N_γ varies between 38 and 192 in different 2D methods.

As previously described, no theoretical solutions for 3D bearing capacity under seismic conditions were found in the literature. Therefore, here the comparisons are made with the other methods only for 2D state and 3D static loading conditions. For more validation, the results of DEM in static loading conditions in 2D and 3D states can be found elsewhere [26, 29, 32].

To compare the statically 3D bearing capacity coefficients (N'_γ, N'_q, N'_c) resulting from other methods with DEM, the result of two classic semi-empirical methods which are extensively used for the shape factors, namely presented by Meyerhof [1] and Hansen [3], and two latest solutions of 3D bearing capacity of foundations obtained by the slices method (Narita and Yamaguchi [12]) and the upper-bound approach of limit analysis (Michalowski [13]) are presented in Figs. 10 to 12 for $\phi = 30°$. The proposed method gives results which are more in accordance with classical semi-empirical 3D bearing capacity coefficients such as Meyerhof [1] and Hansen [3], which are based on the test results carried out by Golder [6] and some additional unpublished data.

In Fig. 13, the comparison of the seismic 2D bearing capacity coefficients related to soil weight ($N_{\gamma,dyn.}$) with those obtained from the other methods for $\phi = 30^{\circ}$ are presented. In addition, comparison of the seismic 2D bearing capacity coefficients related to soil surcharge ($N_{q,dyn.}$) and cohesion ($N_{c,dyn.}$) are respectively presented in Figs. 14 and 15. As can be seen from these figures, the values obtained by DEM are comparatively smaller than other methods. Moreover, the relationship between the seismic 2D bearing capacity coefficients with earthquake horizontal acceleration can be approximately expressed by a linear function.

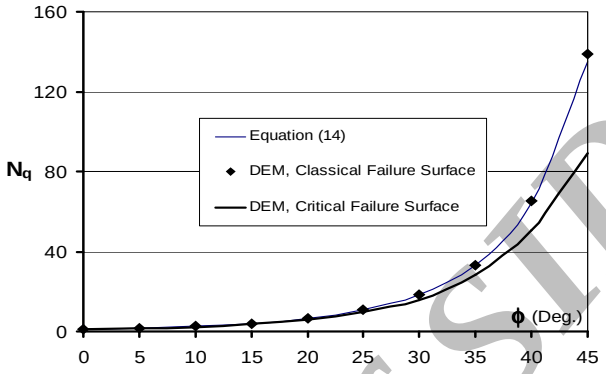

Fig. 7. Comparison of exact mathematical values of N_q and 3D DEM in 2D state

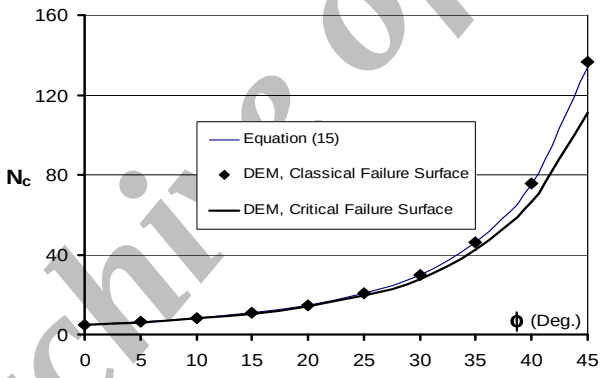

Fig. 8. Comparison of exact mathematical values of N_c and 3D DEM in 2D state

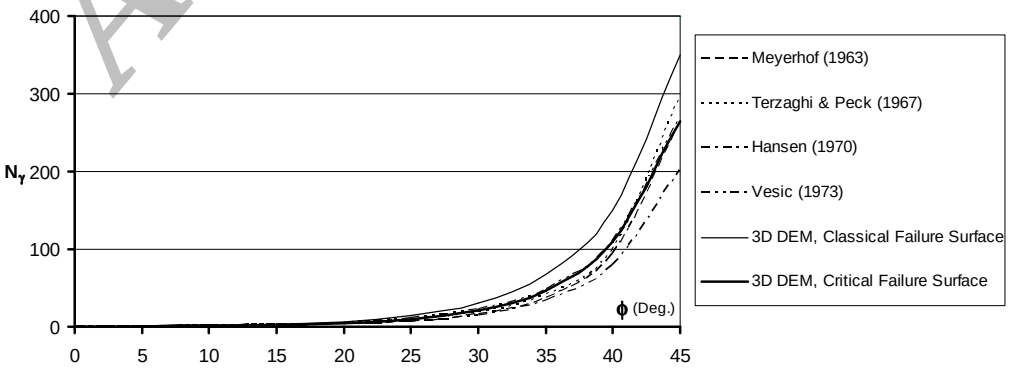

Fig. 9. Comparison of N_γ obtained from conventional methods and 3D DEM in 2D state

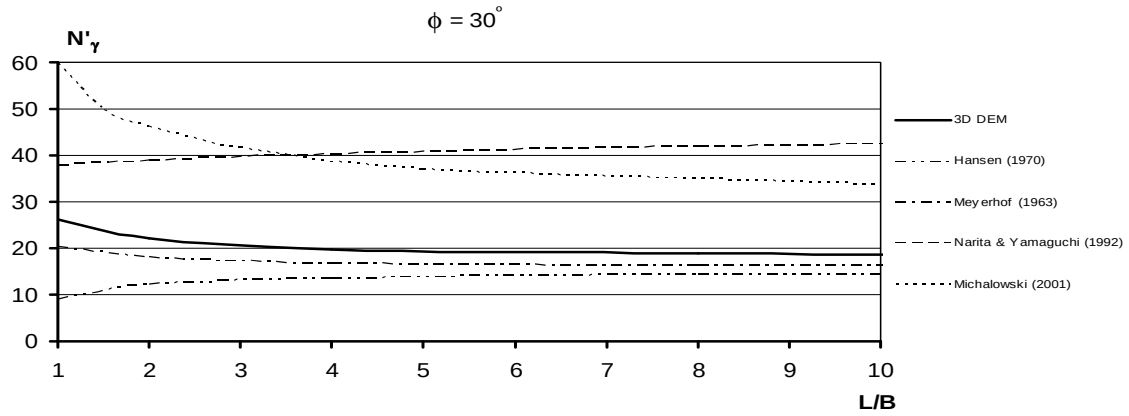

Fig. 10. Comparison of N'_{γ} obtained from various methods for $\phi = 30^{o}$

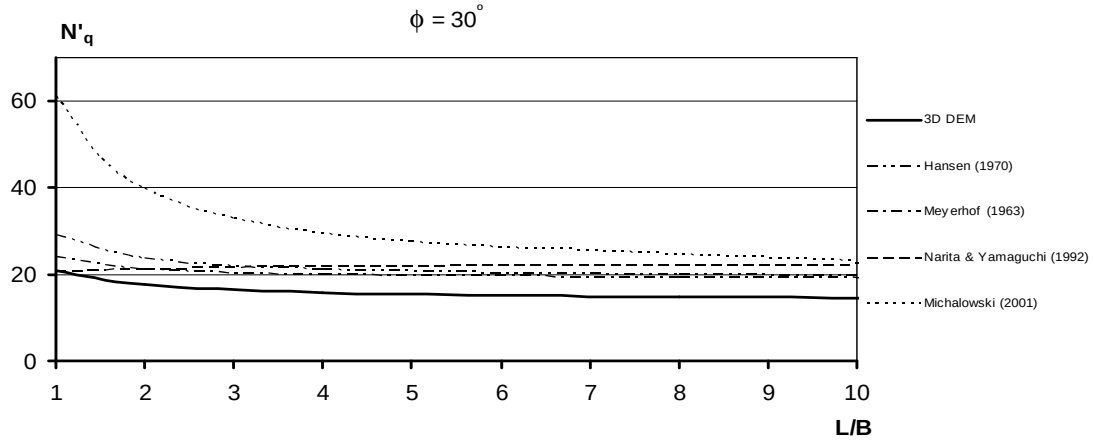

Fig. 11. Comparison of N'_{q} obtained from various methods for $\phi = 30^{\circ}$

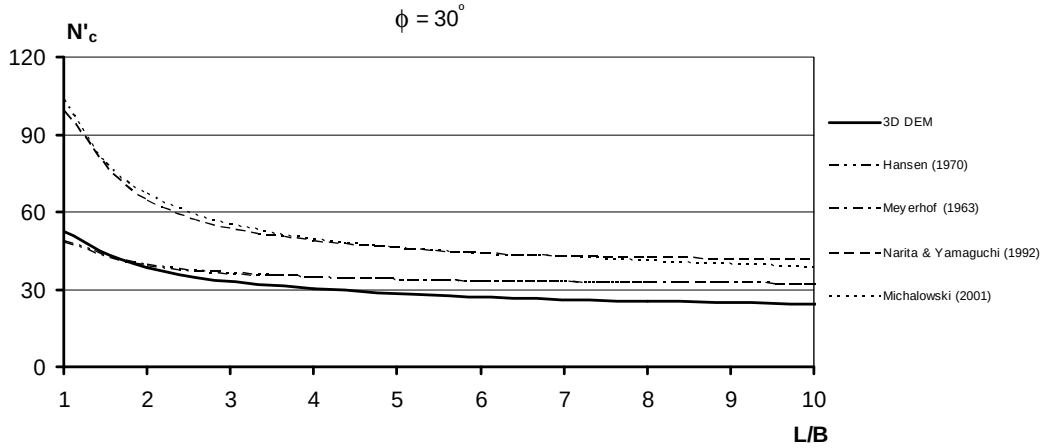

Fig. 12. Comparison of N'_{c} obtained from various methods for $\phi = 30^{\circ}$

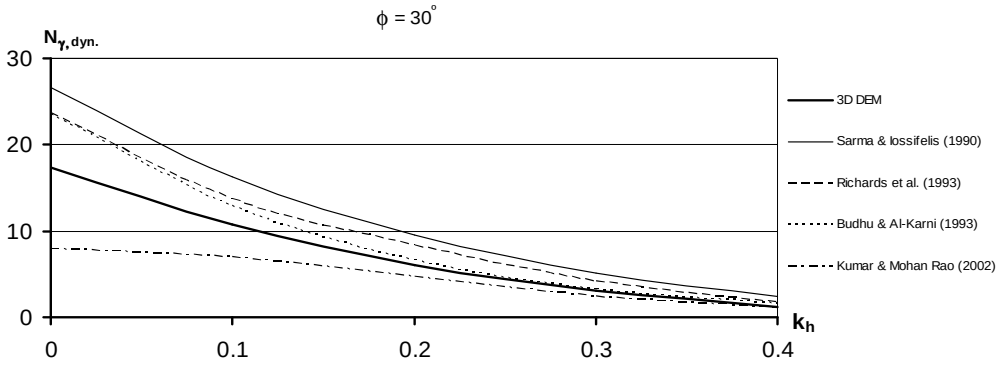

Fig. 13. Comparison of seismic 2D bearing capacity coefficients related to soil weight ($N_{\gamma,dyn.}$) in various methods ($\phi = 30^{\circ}$)

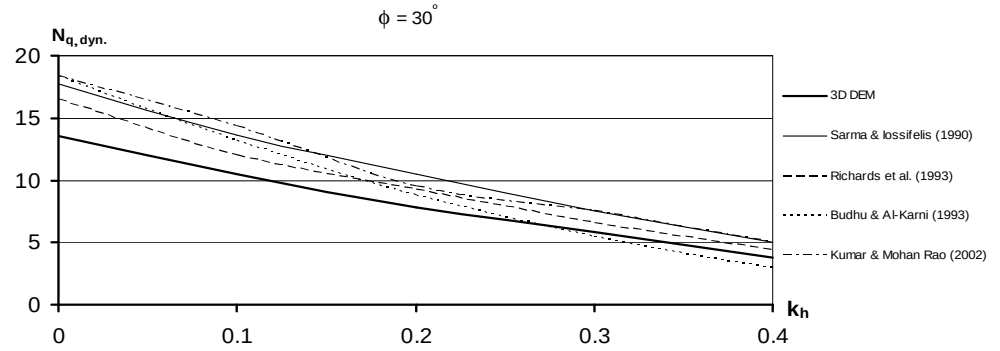

Fig. 14. Comparison of seismic 2D bearing capacity coefficients related to soil surcharge ($N_{q,dyn.}$) in various methods ($\phi = 30^{\circ}$)

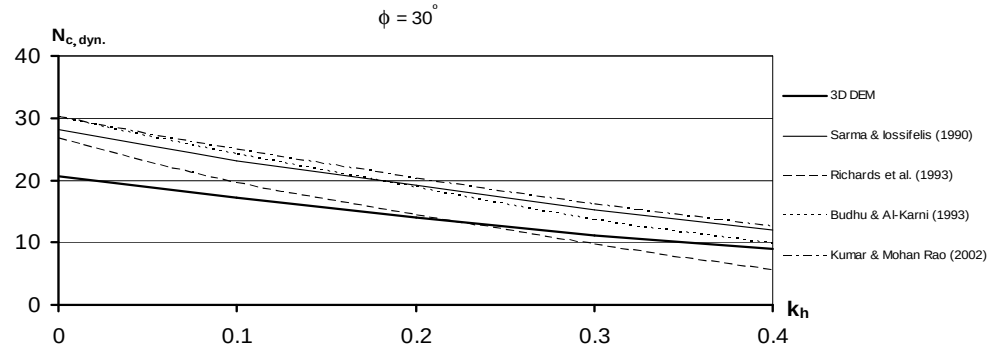

Fig. 15. Comparison of seismic 2D bearing capacity coefficients related to soil cohesion ($N_{c,dyn.}$) in various methods ($\phi = 30^{\circ}$)

b) Pseudo-static 3D bearing capacity coefficients

In Fig. 16, the values of static 3D bearing capacity coefficients related to soil weight (N'_{γ}) for various soil internal friction angles and footing aspect ratios obtained by DEM are presented. Also, in Fig. 17 the values of seismic 3D bearing capacity coefficients related to soil weight ($N'_{\gamma,dyn.}$) for various ϕ and L/B

ratios with an assumption of k_h = 0.3g are shown. As can be seen, the values of $N'_{\gamma,dyn.}$ considerably decrease by increasing the earthquake horizontal acceleration and smoothly decrease by increasing the foundation aspect ratio. Due to linear variations of $N'_{\gamma,dyn.}$ with earthquake horizontal acceleration, only the graphs related to k_h = 0 and k_h = 0.3g are presented and the values of $N'_{\gamma,dyn.}$ related to the other earthquake horizontal accelerations can be simply estimated by interpolation. It is worth mentioning that, in the presentation of these graphs the small values of bearing capacity coefficients (e.g. smaller than 1) are waived.

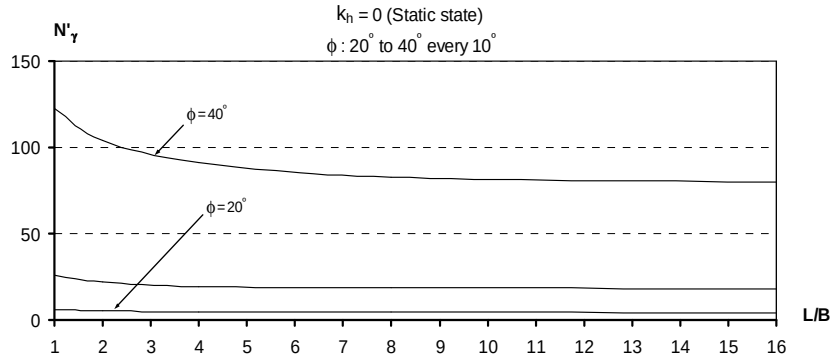

Fig. 16. Static 3D bearing capacity coefficients related to soil weight (N'_{γ}) for various ϕ and L/B ratio obtained by DEM (k_h = 0)

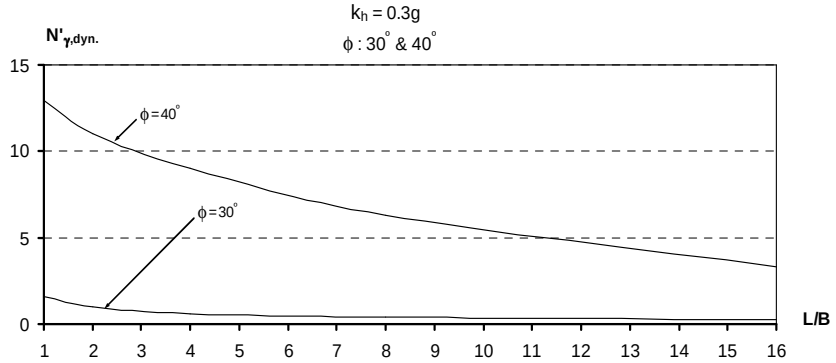

Fig. 17. Seismic 3D bearing capacity coefficients related to soil weight ($N'_{\gamma,dyn.}$) for various ϕ and L/B ratio obtained by DEM (k_h = 0.3g)

In Figs. 18 to 21, the values of static 3D bearing capacity coefficients related to soil surcharge for various ϕ, L/B ratio and k_h obtained by DEM are presented. As can be seen, the curves pertaining to values of $N'_{q,dyn.}$ behave differently for ϕ = 30°, k_h equal to 0.3g and 0.4g, and for ϕ = 40° and k_h equal to 0.2g to 0.4g. It is observed that, for k_h greater than about 0.2g and ϕ greater than about 20° the values of $N'_{q,dyn.}$ increase, first with increasing the L/B up to 2 and then decrease by increasing L/B. In general, the values of bearing capacity coefficients increase with decreasing L/B due to the increase of the contribution of side failure surfaces with respect to overall failure surface. On the other hand, the values of bearing capacity coefficients decrease with increasing k_h. As observed in Figs. 20 and 21, the reduction effects of k_h prevail with respect to increasing the effects of L/B in high values of ϕ and k_h in square footing (L/B=1).

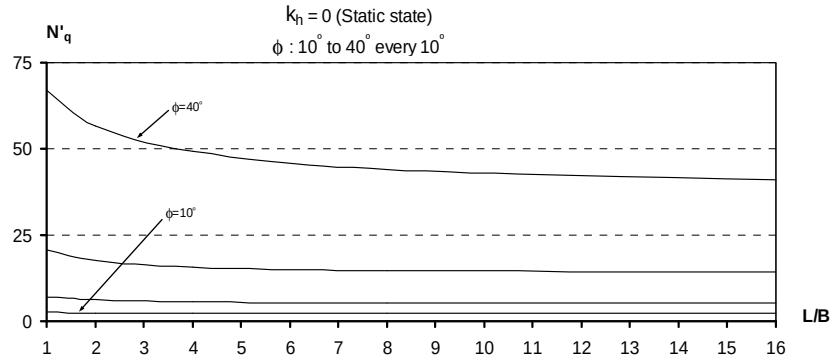

Fig. 18. Static 3D bearing capacity coefficients related to soil surcharge (N'_q) for various ϕ and L/B ratio obtained by DEM (k_h = 0)

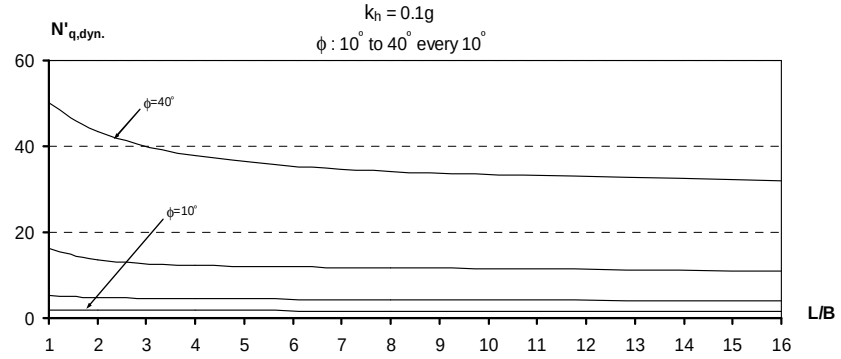

Fig. 19. Seismic 3D bearing capacity coefficients related to soil surcharge ($N'_{q,dyn.}$) for various ϕ and L/B ratio obtained by DEM (k_h = 0.1g)

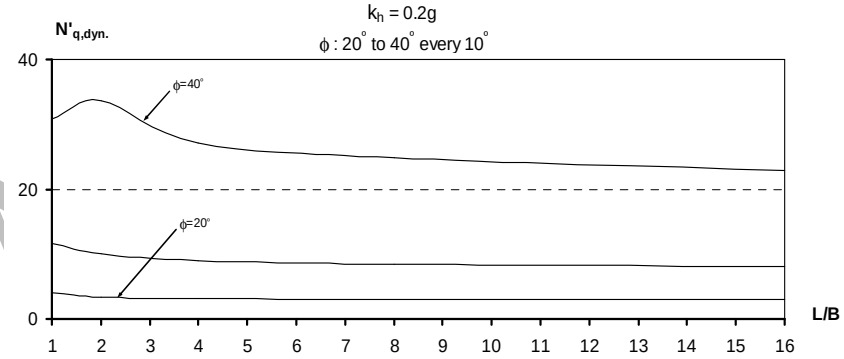

Fig. 20. Seismic 3D bearing capacity coefficients related to soil surcharge ($N'_{q,dyn.}$) for various ϕ and L/B ratio obtained by DEM (k_h = 0.2g)

In Fig. 22, the values of static 3D bearing capacity coefficients related to soil cohesion (N'_c) for various soil internal friction angles and footing aspect ratios obtained by DEM are presented. Also, in Fig. 23 the values of seismic 3D bearing capacity coefficients related to soil cohesion ($N'_{c,dyn.}$) for various ϕ and L/B ratio are obtained with an assumption of k_h = 0.4g. As described previously, the values of $N'_{c,dyn.}$ related to other earthquake horizontal accelerations can be estimated by interpolation. Similar to values of

$N'_{\gamma,dyn.}$, the values of $N'_{c,dyn.}$ considerably decrease by increasing the earthquake horizontal acceleration, while smoothly decreasing as the foundation aspect ratio is increased.

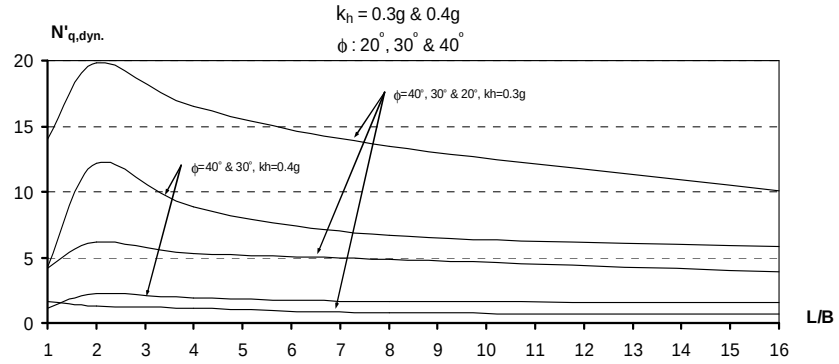

Fig. 21. Seismic 3D bearing capacity coefficients related to soil surcharge ($N'_{q,dyn.}$) for various ϕ and L/B ratio obtained by DEM (k_h = 0.3g & 0.4g)

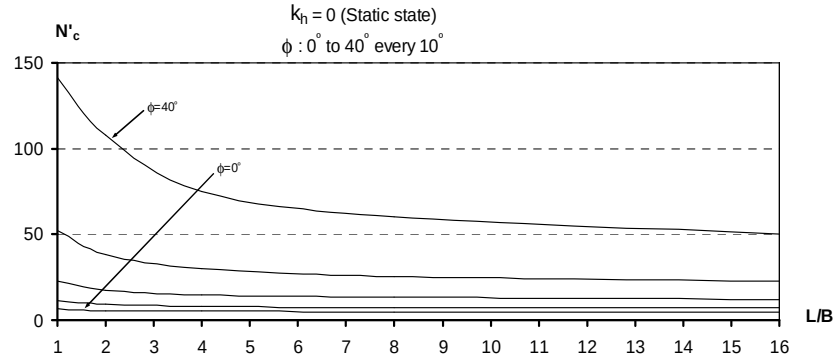

Fig. 22. Static 3D bearing capacity coefficients related to soil cohesion (N'_c) for various ϕ and L/B ratio obtained by DEM (k_h = 0)

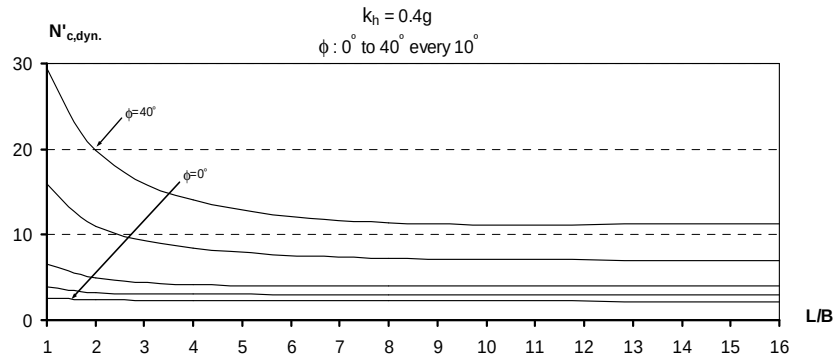

Fig. 23. Seismic 3D bearing capacity coefficients related to soil cohesion ($N'_{c,dyn.}$) for various ϕ and L/B ratio obtained by DEM (k_h = 0.4g)

7. CONCLUSION

In this research, an analysis based on the discrete element method (DEM) is carried out for determining the pseudo-static three dimensional bearing capacity of shallow foundations. The soil mass in the assumed three dimensional failure surface is considered as several discrete blocks connected with Winkler springs. Using an iteration method, the six angles defining the failure surface geometry are independently varied in order to obtain the most critical failure mechanism corresponding to the minimum bearing capacity. The formulation of the method is explained and the pseudo-static bearing capacity coefficients for various internal friction angles and footing aspect ratios are presented. Also, the results are compared with other methods in a 2D state.

The present method is theoretically more rigorous than classical limit equilibrium analyses; it offers more ability in solving bearing capacity problems in complex geometry and loading conditions. The results obtained from the present study can be summarised as follows:

1. The bearing capacity coefficients obtained by DEM are highly dependent on the internal friction of the soil, especially for ϕ amounts greater than 30°.

2. For large internal friction angles the bearing capacity coefficients rapidly increase when the foundation aspect ratio (L/B) drops to 1, whereas for small internal friction angles the amount of increase is much smaller.

3. The N_q and N_c values obtained from exact classical limit solutions are almost identical to DEM results which are obtained with an assumption of classical failure surface angles.

4. The critical values of N_q and N_c in DEM are obviously less than classical exact values for ϕ greater than 30°.

5. The seismic 2D bearing capacity coefficients related to soil weight ($N_{\gamma,dyn.}$), soil surcharge ($N_{q,dyn.}$), and soil cohesion ($N_{c,dyn.}$) obtained by DEM are comparatively smaller than those of the other methods.

6. The relationship between the seismic 2D bearing capacity coefficients with earthquake horizontal acceleration can be expressed by a linear function.

7. In general, the values of seismic 3D bearing capacity coefficients related to soil weight ($N'_{\gamma,dyn.}$), soil surcharge ($N'_{q,dyn.}$) and soil cohesion ($N'_{c,dyn.}$) obtained by DEM, considerably decrease by increasing the earthquake horizontal acceleration and smoothly decrease by increasing the foundation aspect ratio, with the exception of the $N'_{q,dyn.}$, which increases first with increasing L/B for k_h greater than about 0.2g and ϕ greater than about 20°.

***Acknowledgement*:** The work presented in this paper was supported by the College of Engineering, University of Tehran under Grant No. 614-4-1009.

REFERENCES

1. Meyerhof, G. G, (1963). Some recent research on the bearing capacity of foundations. *Can. Geotech. J.*, Vol. 1, No. 1, pp. 16-26.

2. Terzaghi, K. & Peck, R. B. (1967). *Soils mechanics in engineering practice.* J. Wiley, New York.
3. Hansen, J. B. (1970). A revised and extended formula for bearing capacity. *Danish Geotech. Inst. Bulletin*, No. 28, Denmark.
4. De Beer, E. E. (1970). *Experimental determination of shape factors and the bearing capacity factors of sands.* Géotechnique, Vol. 20, No. 4, pp. 387-411.
5. Vesic, A. S. (1973). *Analysis of ultimate loads of shallow foundations. J. of Soil Mech. and Fndn Div., ASCE*, Vol. 99(SM1), pp. 45-73.
6. Golder, H. Q. (1941). *The ultimate bearing pressure of rectangular footings. J. Instn Civ. Engrs*, Vol. 17, No. 2, pp. 161-174.
7. Shield, R. T. & Drucker, D. C. (1953). The application of limit analysis to punch-indentation problems. *J. of Appl. Mech., ASCE*, pp. 453-460.
8. Shield, R. T. (1955). On the plastic flow of metals under conditions of axial symmetry. *Proc. Roy. Soc. of London A*, Vol. 233, pp. 267-287.
9. Cox, A. D., Eason, G. & Hopkins, H. G. (1961). Axially symmetric plastic deformations in soils, *Phil. Trans. Roy. Soc. of London A*, Vol. 254, No. 1036, pp. 1-45.
10. Nakase, A. (1981). Bearing capacity of rectangular footings on clays of strength increasing linearly with depth. *Soils and Foundations*, Vol. 21, No. 4, pp. 101-108.
11. Ugai, K. (1985). Bearing capacity of square and rectangular footings on nonhomogeneous clays. *J. of JSSMFE*, Vol. 25, No. 4, pp. 179-185.
12. Narita, K., Yamaguchi, H. (1992). Three-dimensional bearing capacity analysis of foundations by use of a method of slices. Soils and Foundations. Vol. 32, No. 4, pp. 143-155.
13. Michalowski, R. L. (2001). Upper-bound load estimates on square and rectangular footings. *Géotechnique*, Vol. 51, No. 9, pp. 787-798.
14. Michalowski, R. L., Dawson, E. M. (2002). Three-dimensional analysis of limit loads on Mohr-Coulomb soil. *Fndn of Civ. and Inv. Eng.*, Vol. 1, pp. 137-147.
15. Zhu, M. & Michalowski, R. L. (2005). Shape factors for limit loads on square and rectangular footings. *J. of Geotech. and Geoenv. Eng., ASCE*, Vol. 131, No. 2, pp. 223-231.
16. Salgado, R., Lyamin, A. V., Sloan, S. W. & Yu, H. S. (2004). Two- and three-dimensional bearing capacity of foundations in clay. *Géotechnique*, Vol. 54, No. 5, pp. 297-306.
17. Sarma, S. K. & Iossifelis, I. S. (1990). Seismic bearing capacity factors of shallow strip footings. *Géotechnique*, Vol. 40, No. 2, pp. 265-273.
18. Budhu, M. & Al-Karni, A. (1993). Seismic bearing capacity of soils. *Géotechnique*, Vol. 43, No. 1, pp. 181-187.
19. Richards, R., Elms, D. G. & Budhu, M. (1993). Seismic bearing capacity and settlement of foundations. *J. Geotech. Engng Div., ASCE*, Vol. 119, No. 4, pp. 662-674.
20. Doremieux, L. & Pecker, A. (1995). Seismic bearing capacity of foundation on cohesionless soil. *J. Geotech. Engng Div., ASCE*, Vol. 121, No. 3, pp. 300-303.
21. Subra, A. H. (1997). Seismic bearing capacity of shallow strip footings in seismic conditions. *Proc. Instn Civ. Engrs Geotech. Engng*, Vol. 125, pp. 230-241.
22. Subra, A. H. (1999). Upper-bound solutions for bearing capacity of foundations. *J. Geotech. Geoenviron. Engng, ASCE.*, Vol. 125, No. 1, pp. 59-68.
23. Kumar, J. & Mohan Rao, V. B. K., (2002). Seismic bearing capacity factors for spread foundations, *Géotechnique*, Vol. 52, Vol. 2, pp. 79-88.
24. Ghahramani, A. & Berrill, J. B. (1995). Seismic bearing capacity factors by zero extension line method. *Pacific Conf. on Earthquake Engng, Australia*, pp. 147-155.
25. Roscoe, K. H. (1970). The influence of strains in soil mechanics. *Géotechnique*, Vol. 20, No. 2.

26. Chang, C. S. (1991). Discrete element method for bearing capacity analysis. *Comput. Geotech.*, Vol. 12, pp. 273-288.
27. Chang, C. S. (1992). Discrete element method for slope stability analysis. *J. Geotech. Engng*., Vol. 118, 2, pp. 1889-1905.
28. Chang, C. S. (1994). (1994). Discrete element analysis for active and passive pressure distribution on retaining wall. *Compu. Geotech.*, Vol. 16, pp. 291-310.
29. Mirghasemi, A. A. & Majidi, A. R. (2004). Three dimensional bearing capacity analysis of shallow foundations by discrete element method. *Int. Conf. on Geotech. Engng, Beyrouth*, pp. 481-486.
30. Mirghasemi, A. A. & Majidi, A. R. (2005). Three dimensional bearing capacity analysis of shallow foundations adjacent to slopes. *10th Int. Conf. on Civ., Struc. and Environ. Engng. Comp., Rom*, pp. 254-261.
31. Mirghasemi, A. A. & Maleki-Javan, M. (2006). Discrete Element Method Analysis of Retaining Wall Earth Pressure in Static and Pseudo-Static Conditions. *Iranian Journal of Science & Technology, Transaction B, Engineering*, Vol. 30, No. B1, pp. 145-150.
32. Mirghasemi, A. A. & Majidi, A. R. (2002). Static and pseudo-static bearing capacity analysis of shallow foundations by discrete element method. *Proc. of 5th European Conf. of Num. Meth. in Geotech. Engng*, Paris, pp. 337-342.
33. Terzaghi, K. (1943). *Theoretical soil mechanics*. J. Wiley, New York.
34. Bowles, J. E. (1996). *Foundation analysis and design*. 5th edition, McGraw-Hill, New York.